SIViP
DOI 10.1007/s11760-012-0394-1

ORIGINAL PAPER

# Entropy-based image registration method using the curvelet transform

**Md. Mushfiqul Alam · Tamanna Howlader · S. M. Mahbubur Rahman**

Received: 25 February 2012 / Revised: 20 July 2012 / Accepted: 4 October 2012


**Abstract** Registration is a prerequisite for fusion of geometrically distorted images. Traditionally, intensity-based image registration methods are preferred to feature-based ones due to higher accuracy of the former than that of the latter. To reduce computational load, image registration is often carried out using the approximate-level coefficients of a wavelet-like transform. Directional selectivity of the transform and the objective function used for the coefficients play vital roles in the alignment process of images. This paper introduces an image registration algorithm that uses the approximate-level coefficients of the curvelet transform, directional selectivity of which is better than many wavelet-like transforms. A conditional entropy-based objective function is developed for registration using a suitable probabilistic model of the curvelet coefficients of images. Suitability of the probability distribution of the coefficients is validated using a standard method to assess goodness of fit. To align the distorted images, the affine transformation that possesses parameters related to the translation, rotation, scaling, and shearing is used. Extensive experimentations are carried out to test the performance of the proposed registration method considering that the images are synthetically or naturally distorted. Experimental results show that performance of the proposed registration method is superior to existing methods in terms of commonly used performance metrics.

**Keywords** Image registration · conditional entropy · curvelet coefficient

## 1 Introduction

In the area of visual signal processing, a single image is very often obtained by integrating a number of images so that the information content of this integrated image is higher than that of the individual images. Examples of integration of images include the fusion of multimodal, multitemporal or multisensored source images in the applications of remote sensing [1–3], medical imaging [4–7], navigation and security purposes [8], and product quality assessments in an industrial assembly line [9,10]. Existence of geometric misalignments among these source images is common in practice. The misalignments may arise due to the spatial difference in the locations of the image capturing devices or due to the movements of the target objects. The success of integration of images is highly dependent on the spatially overlaying process of the geometrically misaligned source images. Thus, the process of alignment, which is very often referred to as 'image registration', has become the mandatory first step for the integration of source images. Registration of

Md. M. Alam
School of Electrical and Computer Engineering, Oklahoma State University, 202 Engineering South, Stillwater, OK 74078-5032, USA
e-mail: mdma@okstate.edu

T. Howlader
Institute of Statistical Research and Training, Dhaka University, Dhaka 1000, Bangladesh
e-mail: tamanna@isrt.ac.bd

S. M. M. Rahman (✉)
Department of Electrical and Electronic Engineering, Bangladesh University of Engineering and Technology, Dhaka 1000, Bangladesh
e-mail: mahbubur@eee.buet.ac.bd

*Present address:*
S. M. M. Rahman
Edward S. Rogers Sr. Department of ECE, University of Toronto, 40 St. George Street, BAHEN Bld. Room 4154, Toronto, ON M5S 2E4, Canada

Published online: 27 October 2012

images is also inevitable for the construction of panoramic images from multiview source images [11] and production of 3D scene from multifocused images [12]. Hence, it is an emerging necessity to develop an automatic image registration algorithm that will result in an accurate spatial overlaying of images. Such an algorithm is desired to be computationally efficient, especially when a huge volume of data is needed to be overlaid with a significant level of accuracy and within a short period of time. Traditionally, registration of images is done using one of the two approaches, namely intensity-based [4,13–19] and feature-based [20–25].

In general, the accuracy provided by the intensity-based methods is higher than that provided by the feature-based methods, because pixel values of the entire images are considered in the former instead of a few feature points in the latter. Due to this higher accuracy, the intensity-based registration methods are very often preferred to the feature-based methods. Although an intensity-based registration algorithm can be applied to a number of images, only two images, namely the reference-image and sensed-image, are considered at a time for the geometric alignment. The sensed-image is registered with respect to the reference-image using a suitable geometric mapping function chosen by observing the distortions between these images. A popular choice is the linear mapping function, viz. the affine transform [26] that contains different distortion parameters such as for the rotation, translation, scaling, and shearing. The mapping function may also be chosen as piecewise-linear, polynomial, barrel or pin-cushion type [27] for an arc- or curve-type distortion in images. In order to register the images using the mapping function, an objective function is required. The parameters of the mapping function are usually estimated by optimizing this objective function. Among the existing objective functions that have been used in the intensity-based image registration methods, the cross-correlation [21,28,29], mutual information [8,14–16,18,30–33], joint- and cross-entropies [34], alpha-entropy [35], and Cauchy–Schwartz quadratic distance [36] are worth mentioning. The key problem of cross-correlation-based image registration methods is that such an objective function gives unwanted maxima of correlation while finding the distortion parameters, especially if the pixel intensities of the images have a periodic nature. Wells et al. [33] maximized the mutual information between reference- and sensed-images in terms of the entropies those are calculated using a numerical approximation with a consideration of the Parzen window. Since the reference- and the sensed-images are captured from the same scene, it is expected that the pixel intensities of these images carry a significant level of dependencies. The objective functions that are based on the mutual information and joint entropy ignore the conditional dependencies that may exist in the images to be registered. In [34], the image registration was done using the cross-entropy, which actually measures the conditional entropy between the pixels of the reference- and sensed-images in an indirect way. Further, in these methods, the probability density functions (PDFs) [37] that are necessary for calculating these objective functions are not mentioned explicitly but rather they are chosen heuristically without any justification.

In general, the image registration is carried out in a suitable transform-domain instead of the pixel-domain to take advantages of the properties of the transformations and thus improve the efficiency of the registration methods. For example, an intensity-based image registration method that uses the coefficients of the approximate subband of any of the existing multiscale transformations significantly reduces the computational load as compared to that of a pixel-based method. Among various multiscale transformations, the discrete wavelet transform (DWT)-based [38] registration methods are explored widely and have shown a good performance in the context of accuracy and processing time [18,19,39,31,40]. But, the DWT can capture the edge and ridge features of an image in only four directions, viz. 0°, 90°, and ±45°, and thus suffers from poor directional selectivity. It is noted that the DWT quantifies the directional information of geometric objects in an image from the captured signals and thus does not consider the sensor or position of imaging devices [38]. To improve the directional selectivity of the wavelet transforms, the complex wavelet transform (CWT) that can capture edge features of images in six directions, viz. ±15°, ±45°, and ±75°, was introduced [41,42] and applied for image registration [14]. Nevertheless, the effort to develop computationally efficient wavelet-like transforms that possess improved directional selectivity has never stopped. In this regard, Cnades and Donoho proposed an anisotropic geometric wavelet transform which was named as the ridgelet transform [43,44] that can detect the straight-line singularities. To analyze curve singularities in an image, they proposed to apply the ridgelet transform on the subimages [45]. Later, a formal version of the curvelet transform was developed using the frequency partition technique and mirror extensions of wavelet filters [46–48], and thereafter, this transform was used for image fusion in [49]. To the best of the knowledge of the authors, a significant level of study has not yet been made regarding the use of curvelet transform for the purpose of registration of images.

In this paper, a new image registration algorithm is developed for single-modal or multimodal images by using the coefficients of the approximate subband of the curvelet transform of images. Since the curvelet coefficients of the reference- and sensed-images to be registered possess dependencies, the conditional entropy is used as the objective function for optimizing the mapping function. The suitability of the PDF used for obtaining the conditional entropy is validated using a standard method to assess goodness

of fit. Experimental results show that the proposed image registration method is superior to the existing methods in terms of commonly used performance metrics.

The paper is organized as follows. In Sect. 2, a brief introduction of the curvelet transform is given. A suitable PDF for the curvelet coefficients of images and its validity is presented in Sect. 3. In Sect. 4, the proposed curvelet-based registration method is described in detail. Section 5 provides the experimental results to compare the performance of the proposed and existing methods. Finally, conclusion is given in Sect. 6.

## 2 Curvelet transform: a brief introduction

Curvelets are band-limited complex-valued basis functions $\Psi_{\lambda\beta\phi} : \mathbb{R}^2 \to \mathbb{C}$ parameterized in three spaces, viz. the scale ($\lambda \in \mathbb{Z}^1$), location ($\beta \in \mathbb{Z}^2$), and rotation ($\phi \in \mathbb{S}^1$). Let $I(x, y) \in L_2(\mathbb{R}^2)$ be a pixel value of an image of size $X \times Y$ at the spatial index $(x, y)$. This square integrable function $I(x, y)$ can be represented by discrete version of the forward curvelet transform as [46]

$$\gamma(i, j) = \sum_{\lambda\in\mathbb{Z}^1} \sum_{\beta:(x,y)\in\mathbb{Z}^2} \sum_{\phi:(0,2\pi]\in\mathbb{S}^1} I(i - x, j - y)\Psi_{\lambda\beta\phi} \quad (1)$$

where $\Psi_{\lambda\beta\phi}$ is the basis function for the forward transform. In a similar fashion, the image $I(x, y)$ may be obtained from the coefficients $\gamma(i, j)$ using the inverse curvelet transform as [46]

$$I(x, y) = \sum_{\lambda\in\mathbb{Z}^1} \sum_{\beta:(i,j)\in\mathbb{Z}^2} \sum_{\phi:(0,2\pi]\in\mathbb{S}^1} \gamma(x - i, y - j)\tilde{\Psi}_{\lambda\beta\phi} \quad (2)$$

where $\tilde{\Psi}_{\lambda\beta\phi}$ is the basis function for the inverse transform. A further detail about the history of curvelet transform and relationship of curvelets to other wavelet-like transforms may be found in [50]. An implementation of curvelet transform may be done by using the codes Curvelab version 2.1.2 available at http://www.curvelab.org. Figure 1 shows the magnitudes of the coefficients of the 4-level DWT and that of the curvelet transforms using $\lambda = 4$ and $\phi = 16$ on the test image *MRI*. From this figure, it may be seen that for the same level of decomposition, the curvelet transform groups the edge features of the image in a higher number of orientations than the DWT does. Hence, the directional selectivity of the curvelet transform is better than that of the DWT.

## 3 PDF for curvelet coefficients

The coefficients in a subband of any of the multiscale transforms of an image possess a strong intra-scale dependency [51–53]. Hence, in general, a processing of local neighboring coefficients of any of the wavelet-like transforms of an image

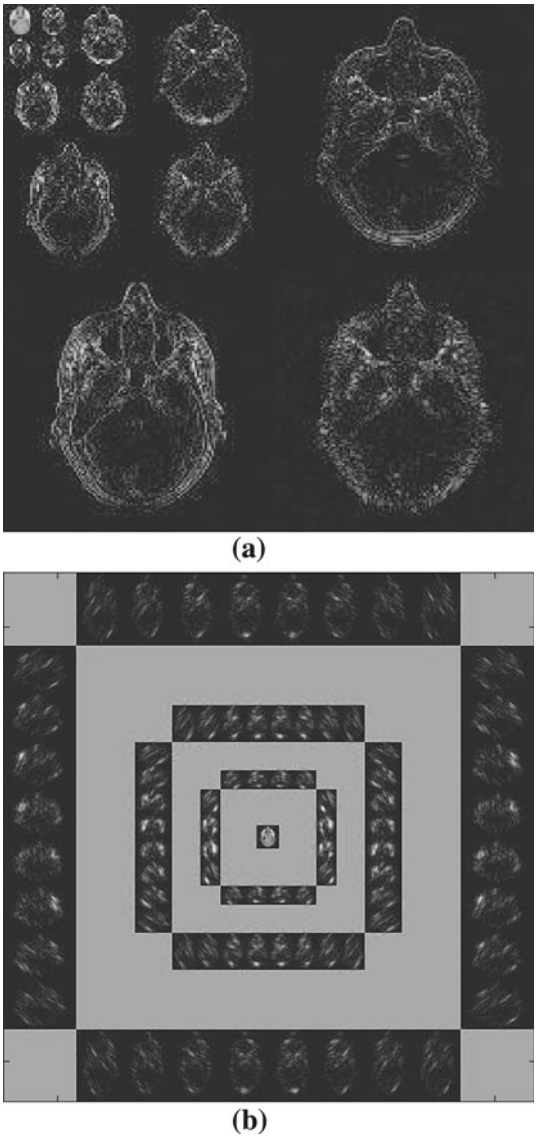

**Fig. 1** Magnitude of the transformed coefficients of the test image *MRI* using **a** a 4-level DWT **b** the curvelet transform ($\lambda = 4, \phi = 16$)

results in better performance as compared to the processing of the coefficients of the entire subband. Being motivated by this fact, we prefer to find a suitable probabilistic model for the local neighboring coefficients of the curvelet transform in the approximate subband that would be used for image registration. The probability model for the coefficients should not only fit the data sufficiently well, but also be mathematically tractable in developing the subsequent image registration algorithm. Let $I_r$ and $I_s$ be the reference- and sensed-images that have to be geometrically overlaid to obtain the registered-images $I_g$. Let $\mathcal{S}(i, j)$ be a square-shaped local window centered at the spatial index $(i, j)$ in the approximate subband of the curvelet transform of the images. Let the curvelet coefficients of the reference- and sensed-images, viz. $\gamma_r(i, j)$ and $\gamma_s(i, j)$, be the sample values of the

random variables $\Gamma_r(i, j)$ and $\Gamma_s(i, j)$, respectively. If not stated otherwise, hereafter in this paper, the index $(i, j)$ will be suppressed for notational convenience. Since the images $I_r$ and $I_s$ are captured from the same scene, it is expected that a strong dependency will exist between the random variables $\Gamma_r$ and $\Gamma_s$. Hence, it is necessary to choose a suitable joint PDF $p_{\Gamma_r\Gamma_s}(\Gamma_r, \Gamma_s)$ for the local neighboring curvelet coefficients of the approximate subband. It is to be noted that the Gaussian PDF is very often chosen as the probability model for local neighboring coefficients of the DWT [52,54] as well as the CWT [55,56] for images. Hence, we choose the joint PDF for the local neighboring curvelet coefficients of the reference- and sensed-images to be the bivariate Gaussian PDF given by [37]

$$p_{\mathbf{\Gamma}}(\mathbf{\Gamma}) = \frac{1}{2\pi\sqrt{|\mathbf{\Sigma}_2|}} \exp\left[-\frac{1}{2}(\mathbf{\Gamma}-\boldsymbol{\mu})^T \mathbf{\Sigma}_2^{-1}(\mathbf{\Gamma}-\boldsymbol{\mu})\right] \quad (3)$$

where $\mathbf{\Gamma} = [\Gamma_r, \Gamma_s]^T$ be the vector containing the random variables $\Gamma_r$ and $\Gamma_s$, and $\boldsymbol{\mu}$ and $\mathbf{\Sigma}_2$ be the mean vector and covariance matrix, respectively. In order to assess the goodness of fit of the proposed PDF with the probabilistic model of the local neighboring curvelet coefficients, we construct chi-square plots by graphing the squared Mahalanobis distance (SMD) denoted as $(\mathbf{\Gamma}-\boldsymbol{\mu})^T \mathbf{\Sigma}_2^{-1}(\mathbf{\Gamma}-\boldsymbol{\mu})$ against the $\chi^2$ quantiles [57]. It is known that the estimated SMD will follow the $\chi^2$ distribution with two degrees of freedom provided the set of data follows the bivariate Gaussian PDF [57]. In other words, the SMDs measured for the local neighboring coefficients of the approximate band of the curvelet transform if plotted against the $\chi^2$ quantiles, then the plot should closely follow the tan 45° line. Figure 2 shows a plot of the squared distances measured for the local neighboring curvelet coefficients with respect to the quantiles using a $5 \times 5$ window for the test images *Toy*, *Room*, *SAR*, and *MRI*. From this figure, it may be observed that the SMD versus $\chi^2$ quantile closely follows the tan 45° line, with a percent of squared error being less than 10 %. It is to be noted that similar results are obtained for these images using local windows of different sizes such as $7 \times 7$ or $9 \times 9$ and for other test images. Hence, the bivariate Gaussian PDF may be chosen as a good candidate for the probabilistic model of the local neighboring curvelet coefficients at the approximate subband.

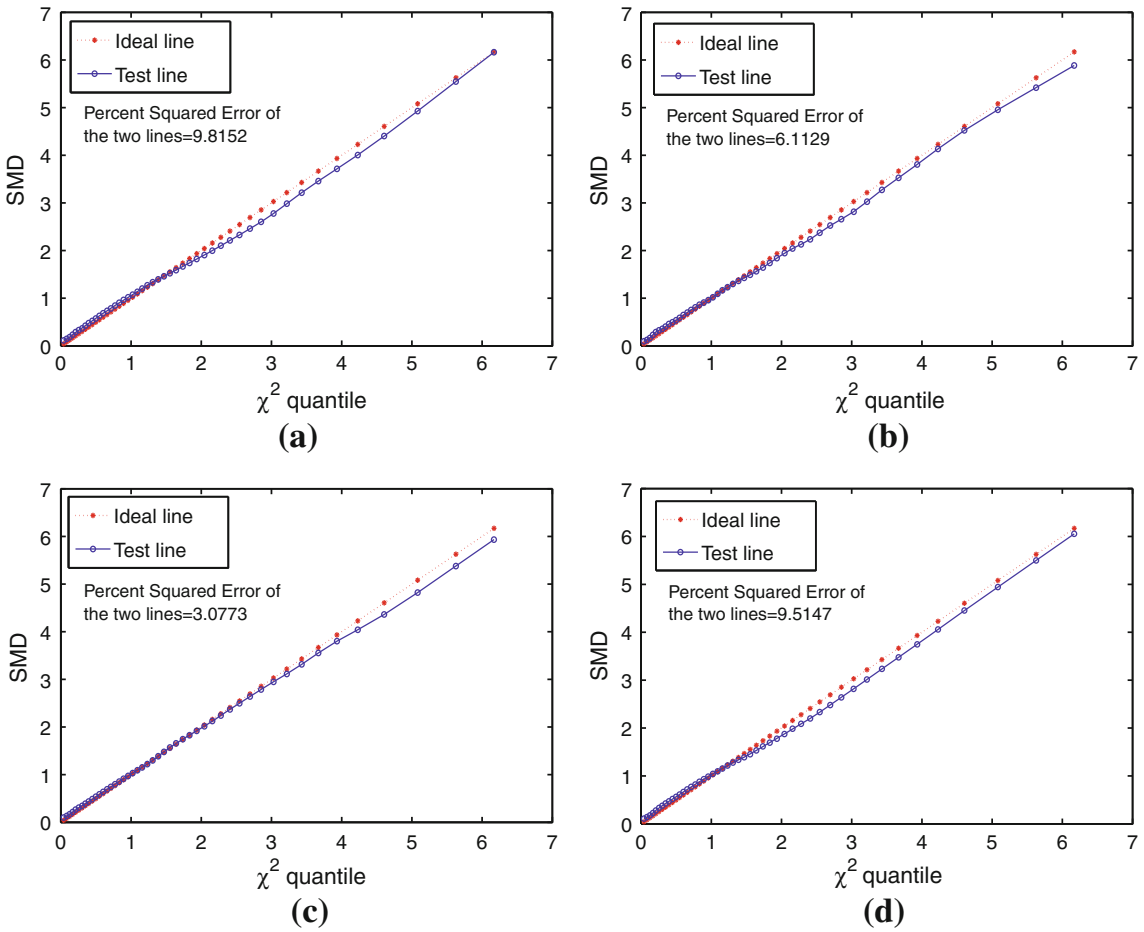


**Fig. 2** SMDs plotted against the $\chi^2$ quantiles for the local neighboring approximate band curvelet coefficients using a $5 \times 5$ window. The images are **a** *Toy*, **b** *Room*, **c** *SAR*, and **d** *MRI*

## 4 Proposed image registration method

In this section, an objective function is derived using the proposed PDF of the curvelet coefficients. The estimation of statistical parameters of the PDF that are required for the objective function is also given. At the end of this section, a summary is provided describing how the distortion parameters of the mapping function for which the objective function is minimized are used for overlaying process of the reference- and sensed-images.

### 4.1 Objective function

In order to derive the objective function, the proposed registration method uses the conditional entropy between the local neighboring curvelet coefficients of the reference- and sensed-images with a consideration that the random variables $\Gamma_r$ and $\Gamma_s$ may have a conditional dependency. Let the conditional entropy $H(\Gamma_s \mid \Gamma_r)$ of the two random variables be expressed as [58]

$$\begin{aligned} &H(\Gamma_s \mid \Gamma_r) \\ &= \int p_{\Gamma_r}(\gamma_r) \left[ -\int p_{\Gamma_s|\Gamma_r}(\gamma_s \mid \gamma_r) \ln p_{\Gamma_s|\Gamma_r}(\gamma_s \mid \gamma_r) \mathrm{d}\gamma_s \right] \mathrm{d}\gamma_r \\ &= -\int\int p_{\Gamma_s\Gamma_r}(\gamma_s, \gamma_r) \ln \left[ \frac{p_{\Gamma_s\Gamma_r}(\gamma_s, \gamma_r)}{p_{\Gamma_r}(\gamma_r)} \right] \mathrm{d}\gamma_s \mathrm{d}\gamma_r \\ &= H(\Gamma_s, \Gamma_r) - H(\Gamma_r) \end{aligned} \tag{4}$$

where $H(\Gamma_s, \Gamma_r)$ is the joint entropy of the random variables $\Gamma_s$ and $\Gamma_r$ given by

$$H(\Gamma_s, \Gamma_r) = -\int\int p_{\Gamma_s\Gamma_r}(\gamma_s, \gamma_r) \ln \left[ p_{\Gamma_s\Gamma_r}(\gamma_s, \gamma_r) \right] \mathrm{d}\gamma_s \mathrm{d}\gamma_r \tag{5}$$

and $H(\Gamma_r)$ is the marginal entropy of $\Gamma_r$ given by

$$H(\Gamma_r) = -\int p_{\Gamma_r}(\gamma_r) \ln \left[ p_{\Gamma_r}(\gamma_r) \right] \mathrm{d}\gamma_r \tag{6}$$

In a similar fashion, the conditional entropy $H(\Gamma_r \mid \Gamma_s)$ may be obtained as

$$H(\Gamma_r \mid \Gamma_s) = H(\Gamma_s, \Gamma_r) - H(\Gamma_s) \tag{7}$$

where $H(\Gamma_s)$ is the marginal entropy of $\Gamma_s$ given by

$$H(\Gamma_s) = -\int p_{\Gamma_s}(\gamma_s) \ln \left[ p_{\Gamma_s}(\gamma_s) \right] \mathrm{d}\gamma_s \tag{8}$$

Here, Eqs. (4) and (7) reveal that the conditional entropies are the difference between the joint and marginal entropies. When the sensed-image is geometrically aligned to the reference-image, then the random variable $\Gamma_s$ will approach to $\Gamma_r$, and thus, any of the two conditional entropies would be minimized. Hence, the values of the distortion parameters of the mapping function of the two images that minimizes any of the two conditional entropies may be used for registration. Since the reference- and sensed-images possess a linear dependency as they are captured from the same scene, and a linear mapping function for the geometric alignment process is considered, the objective function of the proposed method is chosen as the minimization of a linear combination of conditional entropies as

$$\mathcal{F}_{sr} = H(\Gamma_s, \Gamma_r) - \alpha H(\Gamma_s) - (1 - \alpha) H(\Gamma_r) \tag{9}$$

where $\alpha$, $(0 \leq \alpha \leq 1)$ is the weight parameter. If the reference-image is given priority over the sensed-image, then $\alpha$ approaches unity. On the other hand, if the sensed-image is given priority, then $\alpha$ approaches to zero. For example, in order for the registration of two images for the purpose of navigation such that one is captured using a CCD camera and other using infrared camera, the former can be given priority to the latter. In general, $\alpha$ may be set as 0.5 to give equal priority to both the reference- and sensed-images.

In Sect. 3, it is shown that the joint PDF of the local neighboring curvelet coefficients in the approximate band of the reference- and sensed-images may be chosen as the bivariate Gaussian PDF. In such a case, the joint entropy of the random variables $\Gamma_s$ and $\Gamma_r$ can be found as [59]

$$H(\Gamma_s, \Gamma_r) = \frac{1}{2} \ln \left[ (2\pi e)^2 |\mathbf{\Sigma}_2| \right] \tag{10}$$

where $|\cdot|$ represents the determinant of the covariance matrix, which is given by

$$\mathbf{\Sigma}_2 = \begin{bmatrix} \sigma_s^2 & \rho_{sr}\sigma_s\sigma_r \\ \rho_{sr}\sigma_s\sigma_r & \sigma_r^2 \end{bmatrix} \tag{11}$$

where $\sigma_s$ and $\sigma_r$, $(\sigma_s \geq 0, \sigma_r \geq 0)$ are the standard deviations of the random variables $\Gamma_s$ and $\Gamma_r$, respectively, and $\rho_{sr}$, $(-1 \leq \rho_{sr} \leq 1)$ is the correlation coefficient between them. The marginal entropies of the random variables $\Gamma_s$ and $\Gamma_r$ may also be obtained as [60]

$$H(\Gamma_s) = \tfrac{1}{2} \left[ \ln(2\pi\sigma_s^2) + 1 \right] \tag{12}$$

$$H(\Gamma_r) = \tfrac{1}{2} \left[ \ln(2\pi\sigma_r^2) + 1 \right] \tag{13}$$

From Eqs. (9)–(13), it is found that the proposed linear combination of the conditional entropies of the curvelet coefficients $\mathcal{F}_{sr}$ may be expressed in terms of the statistical parameters of the bivariate Gaussian PDF, namely $\sigma_s$, $\sigma_r$, and $\rho_{sr}$. It is to be noted that the random variables $\Gamma_s$ and $\Gamma_r$ are index dependent due to the nonstationary nature of the curvelet coefficients. Hence, the ultimate objective function is obtained by summing up the value of $\mathcal{F}_{sr}(i, j)$ for all the curvelet coefficients of the approximate subband. Thus, the proposed objective function is given by

$$\mathcal{G}_{sr} = \frac{1}{2}\sum_{i=1}^{L_x}\sum_{j=1}^{L_y}\Bigg[\ln\Big[(2\pi e)^2|\mathbf{\Sigma}_2(i,j)|\Big] - \alpha\Big[\ln(2\pi\sigma_s^2(i,j))+1\Big] - (1-\alpha)\Big[\ln(2\pi\sigma_r^2(i,j))+1\Big]\Bigg] \tag{14}$$

where $L_x \times L_y$ is the size of the approximate subband of the curvelet coefficients of the images.

### 4.2 Estimation of parameters

In order to evaluate the objective function, it is required that the parameters, namely the mean, variance, and covariance, of the curvelet coefficients at the approximate subband of the reference- and sensed-images are estimated for each of the spatial index $(i, j)$ using a local neighborhood denoted as $\mathcal{S}(i, j)$. For the purpose of estimation, it is assumed that the coefficients inside the local neighborhood $\mathcal{S}(i, j)$ are independent and identically distributed (i.i.d.) in nature. In other words, the means $\mu_r(k, l) = \mu_r(i, j)$ and $\mu_s(k, l) = \mu_s(i, j)$, the variances $\sigma_r^2(k, l) = \sigma_r^2(i, j)$ and $\sigma_s^2(k, l) = \sigma_s^2(i, j)$, and the covariance $\sigma_{sr}(k, l) = \sigma_{sr}(i, j)$ for all $(k, l) \in \mathcal{S}(i, j)$. In such a case, the parameters may be estimated using the maximum likelihood method as [57]

$$\mu_s(i,j) = \frac{1}{M}\sum_{(k,l)\in\mathcal{S}(i,j)}\gamma_s(k,l) \tag{15}$$

$$\mu_r(i,j) = \frac{1}{M}\sum_{(k,l)\in\mathcal{S}(i,j)}\gamma_r(k,l) \tag{16}$$

$$\sigma_s^2(i,j) = \max\left(\frac{1}{M}\sum_{(k,l)\in\mathcal{S}(i,j)}\Big[\gamma_s(k,l)-\mu_s(i,j)\Big]^2, 0\right) \tag{17}$$

$$\sigma_r^2(i,j) = \max\left(\frac{1}{M}\sum_{(k,l)\in\mathcal{S}(i,j)}\Big[\gamma_r(k,l)-\mu_r(i,j)\Big]^2, 0\right) \tag{18}$$

$$\sigma_{sr}(i,j) = \frac{1}{M}\sum_{(k,l)\in\mathcal{S}(i,j)}\Big[\gamma_s(k,l)\gamma_r(k,l) - \gamma_s(k,l)\mu_r(i,j) - \gamma_r(k,l)\mu_s(i,j) + \mu_s(i,j)\mu_r(i,j)\Big] \tag{19}$$

$$\rho_{sr}(i,j) = \min\left(\max\left(\frac{\sigma_{sr}(i,j)}{\sigma_s(i,j)\sigma_r(i,j)}, -1\right), 1\right) \tag{20}$$

where $M$ is the number of coefficients in $\mathcal{S}(i, j)$.

### 4.3 Mapping function

The ultimate target of the proposed method is to geometrically align the sensed-image on the reference-image using a suitable mapping function that is capable of handling common forms of distortions including the scaling, translation, shearing, and rotation. We have considered that the sensed-image to be registered undergoes a combination of linear distortions uniformly. It is to be noted that such a uniform distortion may be applied locally where nonuniform or piecewise-linear distortion is considered. Let a pixel intensity of an estimate of the registered-image, that is, an aligned version of the sensed-image, $\hat{I}_{as}(x', y')$ be obtained from the given sensed-image $I_s(x, y)$ using the affine transformation defined by [26]

$$\begin{bmatrix} x' \\ y' \\ 1 \end{bmatrix} = \begin{bmatrix} \cos\theta & \sin\theta & 0 \\ -\sin\theta & \cos\theta & 0 \\ 0 & 0 & 1 \end{bmatrix} \cdot \begin{bmatrix} c_x & 0 & 0 \\ 0 & c_y & 0 \\ 0 & 0 & 1 \end{bmatrix} \cdot \begin{bmatrix} 1 & s_h & 0 \\ 0 & 1 & 0 \\ 0 & 0 & 1 \end{bmatrix} \cdot \begin{bmatrix} 1 & 0 & 0 \\ s_v & 1 & 0 \\ 0 & 0 & 1 \end{bmatrix} \cdot \begin{bmatrix} 1 & 0 & t_x \\ 0 & 1 & t_y \\ 0 & 0 & 1 \end{bmatrix} \cdot \begin{bmatrix} x \\ y \\ 1 \end{bmatrix} \tag{21}$$

where $\theta \in \mathbb{S}^1$, $(c_x, c_y) \in \mathbb{Z}^2$, $(s_h, s_v) \in \mathbb{R}^2$, and $(t_x, t_y) \in \mathbb{Z}^2$ are the rotation, scaling, shearing, and translation parameters, respectively. It is to be noted that the desired set of distortion parameters, that is, $(\hat{\theta}, \hat{c}_x, \hat{c}_y, \hat{s}_h, \hat{s}_v, \hat{t}_x, \hat{t}_y)$, for which $I_g$ is obtained from the aligned versions of the sensed-image such that $I_{as}$ is overlaid on $I_r$ can only be obtained by minimizing the objecting function $\mathcal{G}_{sr}$ given in Eq. (14) through a nonlinear optimization technique. In this regard, $N$ number of geometrically aligned versions of the sensed-image denoted as $I_{as}^n$, $(n = 1, 2, 3, \ldots, N)$ are obtained by using a uniform search grid of distortion parameters $(\theta^n, c_x^n, c_y^n, s_h^n, s_v^n, t_x^n, t_y^n)$, $(n = 1, 2, 3, \ldots, N)$ applied on the given sensed-image $I_s$. Thus, $N$ number of approximate bands of the curvelet transform of aligned versions of the sensed-image denoted as $\mathcal{C}_{As}^n$, $(n = 1, 2, 3, \ldots, N)$ are obtained, wherein each of the subbands corresponds to $I_{as}^n$, $(n = 1, 2, 3, \ldots, N)$. On the other hand, only one approximate subband of curvelet coefficients denoted as $\mathcal{C}_{Ar}$ is obtained for the reference-image $I_r$. Thus, the set of distortion parameters $(\theta^n, c_x^n, c_y^n, s_h^n, s_v^n, t_x^n, t_y^n)$, $(n = 1, 2, 3, \ldots, N)$ of the sensed-image would result in $N$ number of values for the objective function $\mathcal{G}_{sr}^n$, $(n = 1, 2, 3, \ldots, N)$ using the approximate subbands $\mathcal{C}_{As}^n$, $(n = 1, 2, 3, \ldots, N)$ and $\mathcal{C}_{Ar}$. In the proposed method, the registered-image $I_g$ is considered to be the geometrically aligned version of the sensed-image $\hat{I}_{as}$ corresponding to the parameters $(\hat{\theta}, \hat{c}_x, \hat{c}_y, \hat{s}_h, \hat{s}_v, \hat{t}_x, \hat{t}_y)$, when $\mathcal{G}_{sr}^n$, $(n = 1, 2, 3, \ldots, N)$ becomes minimum, which can mathematically be shown as

$$\begin{aligned} I_g &= \hat{I}_{as}(\hat{\theta}, \hat{c}_x, \hat{c}_y, \hat{s}_h, \hat{s}_v, \hat{t}_x, \hat{t}_y) \\ &= \arg\min_{I_{as}^n(\theta^n, c_x^n, c_y^n, s_h^n, s_v^n, t_x^n, t_y^n)} \mathcal{G}_{sr}^n \end{aligned} \tag{22}$$

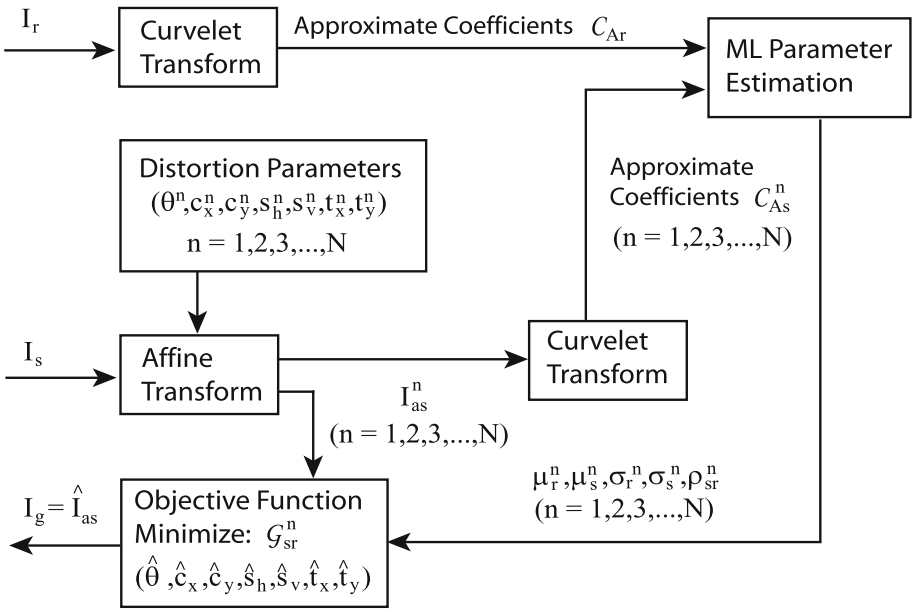


**Fig. 3** A block diagram of the proposed curvelet-based image registration algorithm

**Table 1** Results concerning the performance metrics for registering the sensed-image that is distorted by translation in $x$-axis and shear in horizontal direction

| Images | Methods | Performance Metrics in $10^{-2}$ | | |
|---|---|---|---|---|
| | | NRMSD | NCCC | PRRMSE |
| *Toy* | Method 1 | 8.45 | 25.24 | 0.66 |
| | Method 2 | 15.48 | 21.46 | 0.89 |
| | Method 3 | 9.46 | 25.34 | 0.57 |
| | Proposed | **4.71** | **26.10** | **0.28** |
| *Room* | Method 1 | 65.56 | 0.02 | 2.25 |
| | Method 2 | 75.14 | 12.75 | 2.56 |
| | Method 3 | 65.54 | 0.02 | 2.24 |
| | Proposed | **65.46** | **27.00** | **2.23** |
| *SAR* | Method 1 | 27.37 | 4.30 | 0.88 |
| | Method 2 | 27.85 | 4.30 | 0.92 |
| | Method 3 | 27.35 | 4.31 | 0.88 |
| | Proposed | **23.64** | **6.95** | **0.76** |
| *Tree* | Method 1 | 31.64 | 19.75 | 3.60 |
| | Method 2 | 32.19 | 19.75 | 3.62 |
| | Method 3 | 32.18 | 19.74 | 3.66 |
| | Proposed | **31.49** | **22.59** | **3.58** |
| *MRI* | Method 1 | 12.22 | 18.61 | 2.06 |
| | Method 2 | 21.28 | 10.32 | 3.57 |
| | Method 3 | 12.21 | **18.97** | 2.05 |
| | Proposed | **11.02** | **18.97** | **1.85** |
| *Ship* | Method 1 | 45.92 | 11.47 | 1.59 |
| | Method 2 | 43.11 | 12.38 | **1.41** |
| | Method 3 | 43.11 | **14.87** | 1.49 |
| | Proposed | **40.64** | **14.87** | **1.41** |
| *CT-MRI* | Method 1 | 19.11 | 0.29 | 4.50 |
| | Method 2 | 23.22 | 0.39 | 5.47 |
| | Method 3 | 23.24 | 0.16 | 5.48 |
| | Proposed | **18.65** | **0.41** | **4.39** |

**Table 2** Results concerning the performance metrics for registering the sensed-image that is distorted by translation in $x$-axis, translation in $y$-axis, and rotation

| Images | Methods | Performance Metrics in $10^{-2}$ | | |
|---|---|---|---|---|
| | | NRMSD | NCCC | PRRMSE |
| *Toy* | Method 1 | 5.13 | 25.40 | 0.32 |
| | Method 2 | 5.23 | 25.01 | 0.32 |
| | Method 3 | 5.13 | 25.41 | **0.31** |
| | Proposed | **5.12** | **25.43** | **0.31** |
| *Room* | Method 1 | 65.50 | 0.81 | **2.22** |
| | Method 2 | 73.63 | 0.87 | 2.50 |
| | Method 3 | 65.48 | 0.78 | 2.23 |
| | Proposed | **65.46** | **0.88** | **2.22** |
| *SAR* | Method 1 | 14.14 | 5.02 | 0.42 |
| | Method 2 | 14.24 | 5.07 | **0.41** |
| | Method 3 | 14.10 | 5.09 | 0.42 |
| | Proposed | **14.07** | **5.11** | **0.41** |
| *Tree* | Method 1 | 31.34 | 1.78 | 3.78 |
| | Method 2 | 37.62 | 2.01 | 4.20 |
| | Method 3 | 35.42 | 1.74 | 4.02 |
| | Proposed | **30.14** | **2.41** | **3.45** |
| *MRI* | Method 1 | 11.41 | 19.11 | 1.90 |
| | Method 2 | 15.77 | 19.21 | 2.64 |
| | Method 3 | 11.30 | 19.14 | 1.89 |
| | Proposed | **10.87** | **19.28** | **1.82** |
| *Ship* | Method 1 | 46.38 | 12.49 | **1.60** |
| | Method 2 | 46.45 | 12.44 | 1.61 |
| | Method 3 | 46.38 | 12.49 | **1.60** |
| | Proposed | **46.35** | **12.50** | **1.60** |
| *CT-MRI* | Method 1 | **17.65** | **0.41** | **4.16** |
| | Method 2 | 17.66 | 0.40 | **4.16** |
| | Method 3 | **17.65** | **0.41** | **4.16** |
| | Proposed | **17.65** | **0.41** | **4.16** |

**Table 3** Absolute error in estimating the angle of rotation $|\Delta\theta|$ for image sets using different methods

Actual parameter value of rotation is $\theta = 0.37$ radian counterclockwise for the image sets

| Images | Method 1 | Method 2 | Method 3 | Proposed |
|---|---|---|---|---|
| *Toy* | 0.0035 | 0.0031 | 0.0035 | **0.0030** |
| *Room* | 0.0052 | 0.0026 | 0.0048 | **0.0019** |
| *SAR* | 0.0048 | 0.0122 | 0.0048 | **0.0042** |
| *Tree* | **0.0005** | 0.0104 | **0.0005** | **0.0005** |
| *MRI* | 0.0031 | 0.0078 | 0.0031 | **0.0005** |
| *Ship* | 0.0013 | 0.0004 | 0.0013 | **0.0000** |
| *CT-MRI* | 0.0122 | 0.0048 | 0.0122 | **0.0005** |

A simple block diagram of the proposed image registration method is shown in Fig. 3. It is to be pointed out that in the proposed method, a number of discrete values of the entire search space of the distortion parameters of the aligned versions of the sensed-image are considered. In practice, however, the global minima of the objective function may be obtained for an optimal registration performance, provided the number of discrete points $N$ is sufficiently high within a specified search region.

## 5 Experimental results

Extensive experimentations have been carried out to test the performance of the proposed image registration algorithm as compared to that of the existing methods. A large number of test images, available at www.imagefusion.org and sources mentioned therein, are first synthetically distorted and then aligned to evaluate the registration performance. Due to space constraints, however, in this section, only the

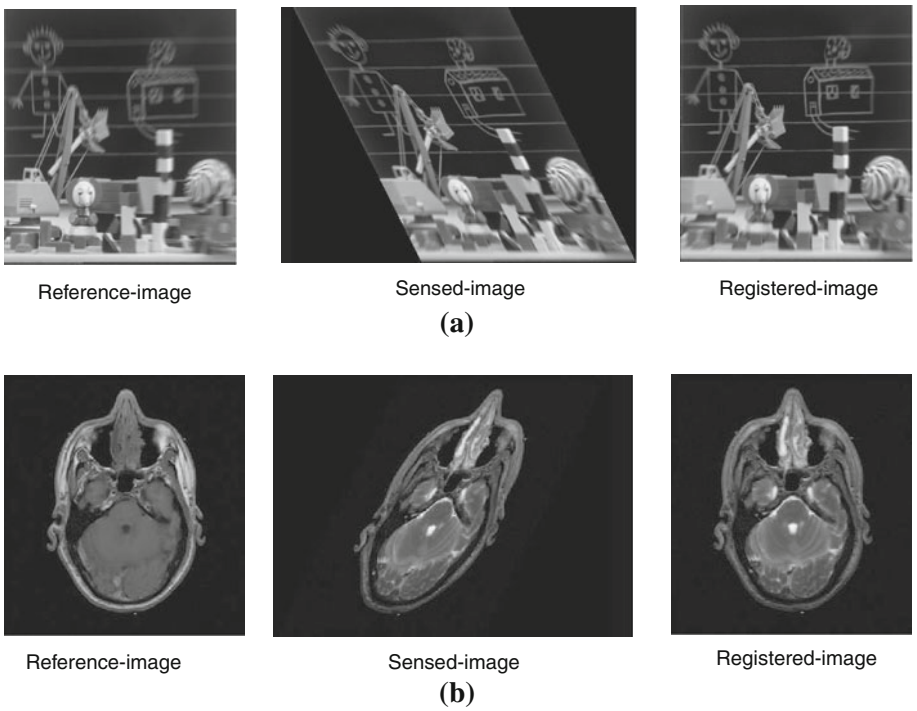


**Fig. 4** Visual outputs of the proposed registration method on the sensed-images that are distorted by a translation in $x$-axis and a shearing in horizontal direction. The images are **a** *Toy*, which is distorted by $t_x = 30$ and $s_h = 0.6$, and **b** *MRI*, which is distorted by $t_x = -30$ and $s_h = -0.6$

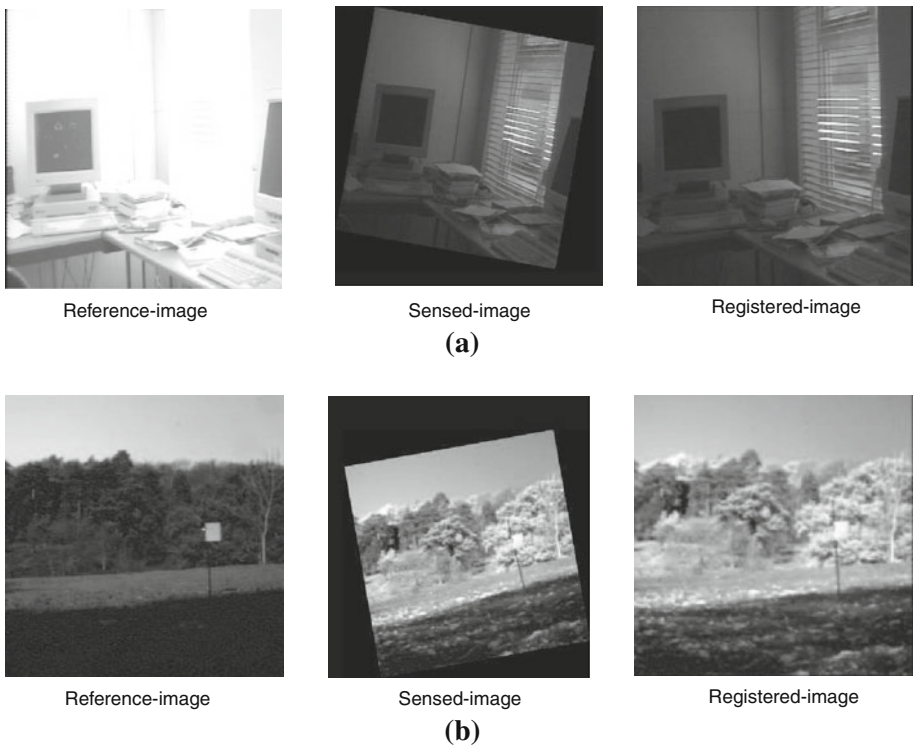


**Fig. 5** Visual outputs of the proposed registration method on the sensed-images that are distorted by a translation in $x$-axis, a translation in $y$-axis, and a rotation. The images are **a** *Room*, which is distorted by $t_x = -20$, $t_y = -40$, and $\theta = 10^\circ$ clockwise, and **b** *Tree*, which is distorted by $t_x = 20$, $t_y = 40$, and $\theta = 10^\circ$ counterclockwise

registration performance on the seven sets of test images, viz. *Toy*, *Room*, *SAR*, *Tree*, *MRI*, *Ship*, and *CT-MRI*, is presented. The reference- and sensed-images of *Toy* are left- and middle-focused, respectively. The test images in the set *Room* are different in exposures of light. The images of the sets *SAR* and *Tree* are captured by sensors with multispectral sensitivity. The reference- and sensed-images of *MRI* are captured by a single imaging device, but in two different modes, namely T1 and T2, respectively. In contrast, the test sets *Ship* and *CT-MRI* consist of images that are

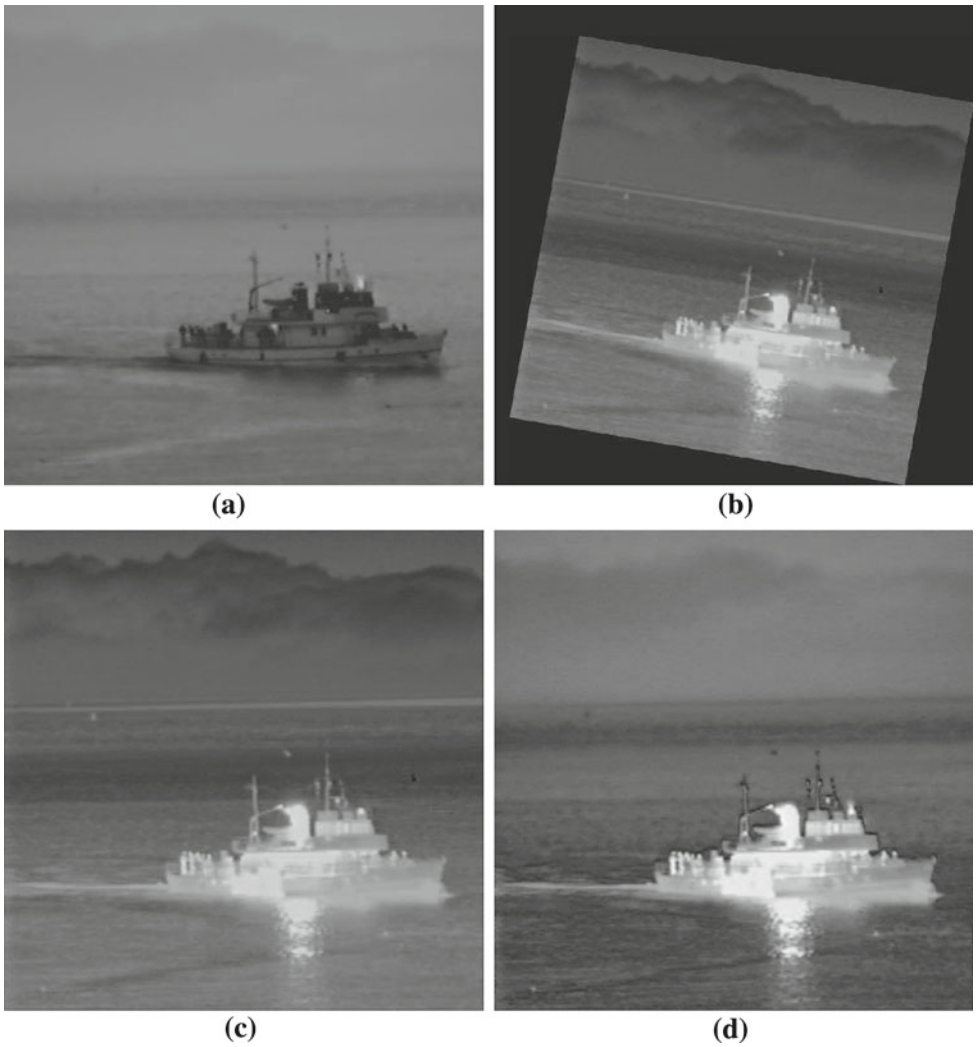


**Fig. 6** Visual outputs of the proposed registration method using the image set *Ship*. The images are **a** reference-image, **b** sensed-image, which is distorted by $t_x = 20$, $t_y = 40$, and $\theta = 10°$ clockwise, **c** registered-image, **d** fused-image obtained using a pixel-by-pixel maximization rule

captured using multiple imaging devices. The reference- and sensed-images of the set *Ship* are captured using the CCD and infrared cameras, respectively. In the case of *CT-MRI*, the CT scan of a brain is considered as the reference-image, whereas the MRI scan as the sensed-image. In the experimentations, it is considered that the sensed-image may be geometrically misaligned due to a single-level distortion as well as multiple-level distortions such as two or three distortions at a time among seven commonly used independent distortions, viz. rotation, scaling in $x$ or $y$ axis, horizontal or vertical shearing, translation in $x$ or $y$ axis. The proposed method is compared with competing three types of intensity-based image registration methods, and significant features of those are briefly described below:

– *Method 1* [18,31]: In this case, the alignment is done through a maximization of the mutual information that exists between the coefficients of the approximate level of the DWT of the reference- and sensed-images.
– *Method 2* [40]: In this method, alignment is done by maximization of the normalized cross-correlation between the thresholded approximate coefficients of the DWT obtained at different levels of the reference- and sensed-images. The approximate coefficients at a given level are thresholded to the 50 % of the maximum value and to the 40 % at the next lower level.
– *Method 3* [8,32]: In these methods, the objective function is the mutual information of the pixel intensities of the reference- and sensed-images.

In order to compare the registration performance of the proposed method with that of these methods, three commonly used performance metrics, namely normalized root mean square distortion (NRMSD), normalized cross-correlation coefficient (NCCC), and percent relative root mean square error (PRRMSE), are used. These performance metrics are estimated using the following relations [61,62]:

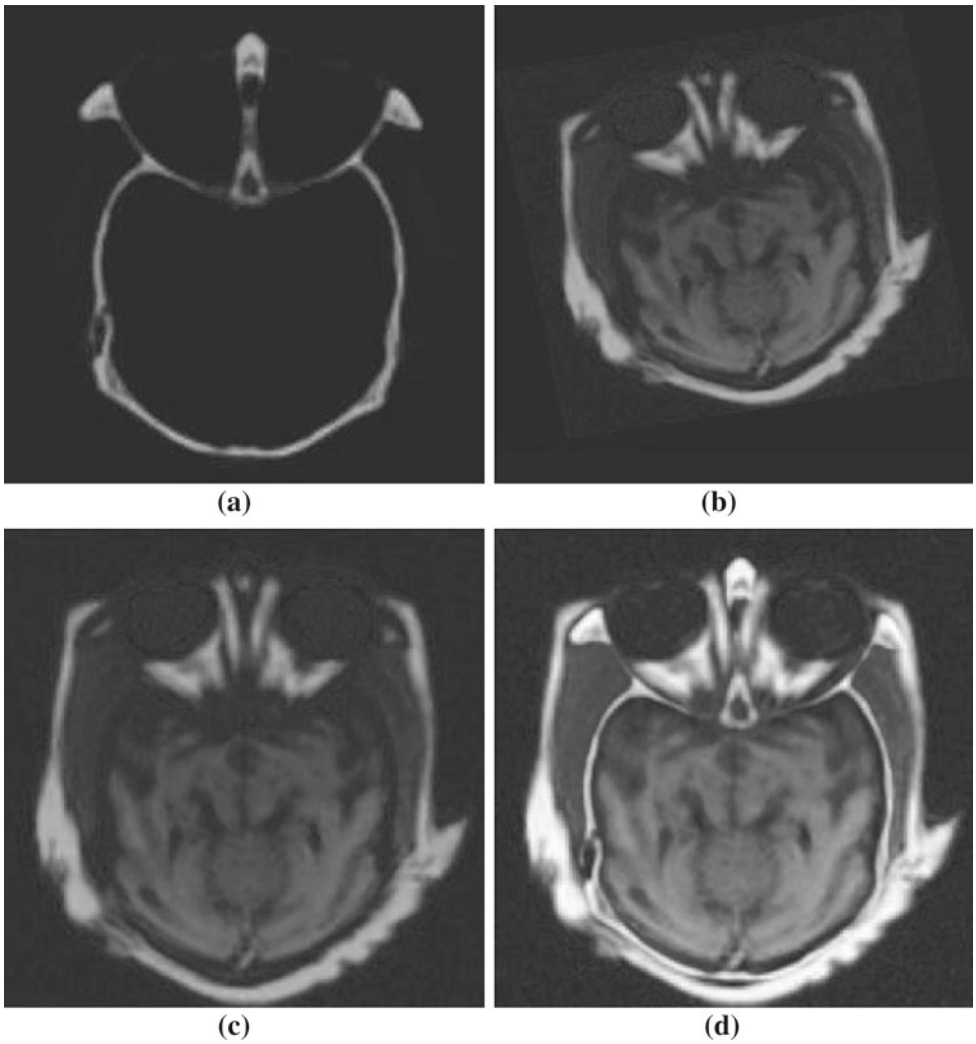


**Fig. 7** Visual outputs of the proposed registration method using the image set *CT-MRI*. The images are **a** reference-image, **b** sensed-image, which is distorted by $t_y = -30$ and $\theta = 10°$ counterclockwise, **c** registered-image, **d** fused-image obtained using a pixel-by-pixel maximization rule

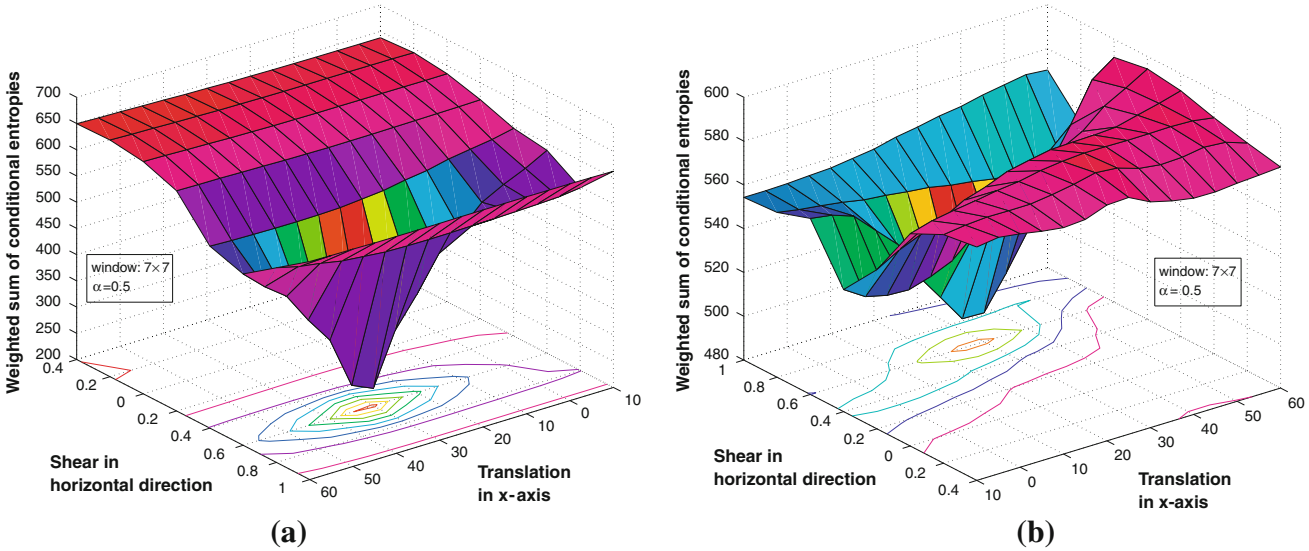


**Fig. 8** The surface of the proposed objective function in the case of registration of sensed-images that are distorted by a translation in $x$-axis and a shearing in horizontal direction. The objective functions correspond to the images **a** *Toy*, when the function is minimized at $t_x = -30$ and $s_h = -0.6$, and **b** *MRI*, when the function is minimized at $t_x = 30$ and $s_h = 0.6$


**Fig. 9** Visual output of a geometric alignment process using the proposed registration method on a real SAR image by utilizing a clockwise rotation of 15°

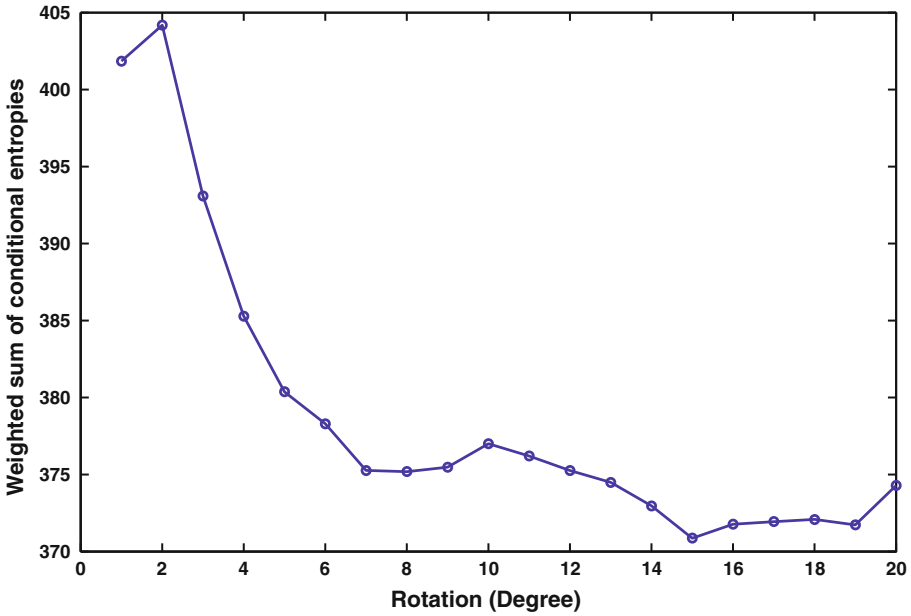


**Fig. 10** The proposed objective function that utilizes the clockwise rotation for registration of the real SAR image

$$\text{NRMSD} = \sqrt{\frac{\sum_{x=1}^{X}\sum_{y=1}^{Y}\left(I_r(x,y) - I_g(x,y)\right)^2}{XY(I^r_{\max} - I^r_{\min})}}$$

$$\text{NCCC} = \frac{\sum_{x=1}^{X}\sum_{y=1}^{Y}\left(I_r(x,y) - \bar{I}_r\right)\left(I_g(x,y) - \bar{I}_g\right)}{\sqrt{\sum_{x=1}^{X}\sum_{y=1}^{Y}\left(I_r(x,y) - \bar{I}_r\right)^2\left(I_g(x,y) - \bar{I}_g\right)^2}}$$

$$\text{PRRMSE} = \sqrt{\frac{\sum_{x=1}^{X}\sum_{y=1}^{Y}\left(I_r(x,y) - I_g(x,y)\right)^2}{XY\sum_{x=1}^{X}\sum_{y=1}^{Y} I_r(x,y)}}$$

where $I^r_{\max}$ and $I^r_{\min}$ are the maximum and minimum pixel intensities of the reference-image, and $\bar{I}_r$ and $\bar{I}_g$ are the mean values of pixel intensities of the reference- and registered-images, respectively. The NRMSD and PRRMSE are the measures of distortions that may remain between the registered- and reference-images. This is due to the fact that the pixel intensities of the reference- and sensed-images of a same scene are dissimilar in general, and hence, distortions may exist even though they are geometrically aligned perfectly. However, the higher the accuracy of the alignment process of the two images through a registration algorithm, the lower the values of the NRMSD and PRRMSE will be. On the other hand, the NCCC is a measure of closeness of the reference- and registered-images. Hence, a higher value of the NCCC indicates a higher accuracy in the overlaying process.

Tables 1 and 2 show the results obtained for the four types of image registration methods and seven sets of test images considered in the experiments while the sensed-images are distorted by translation in $x$-axis and horizontal shearing ($t_x = 30, s_h = 0.6$), and translations in $x$- and $y$-axes and rotation ($t_x = 30, t_y = 40, \theta = 10°$, clockwise), respectively. The curvelet transform of the proposed method uses $\lambda = 4$ and $\phi = 16$, and a 4-level decomposition is used for the DWT-based methods. In order to estimate the statistical parameters for the objective function of the proposed method, the square-shaped local window $\mathcal{S}$ is chosen as $7 \times 7$. In Tables 1 and 2, the results that are best for the image

registration in terms of the NMRSD, NCCC, and PRRMSE are shown in boldface. It is to be noted that the results remain similar, when a different window size such as $5 \times 5$ or $9 \times 9$ is chosen for the parameter estimation, and those are not shown due to space constraints. An observation on the values given in the two tables reveals that the proposed method provides the best results in terms of the commonly used performance metrics as compared to the other methods. In a few instances, the proposed method shows a similar performance as the other methods do, but the performance of former is never inferior to that of the latter. Hence, considering the overall performance, it can be concluded that the proposed method outperforms the existing image registration methods.

The proposed method is also compared with the other methods in terms of the absolute error in estimating the registration parameters. Table 3 shows the absolute error in estimating the rotation parameter denoted as $|\Delta\theta|$ for the seven synthetically distorted sensed-images using the parameter $\theta = 0.37$ radian counteclockwise. It can be seen from this table that the error in estimation, measured as the absolute difference between the ground-truth and estimated value of the angle of rotation, although small is minimum for the proposed method as compared to the other methods. Similar results are observed for other registration parameters, but are not shown due to the space limitation. It should be noted that even a small improvement in the accuracy of estimating the registration parameter cannot be ignored, especially for further processing such as fusion of the registered- and reference-images.

Figure 4 shows visual outputs of the reference images *Toy* and *MRI*, synthetically generated sensed versions of the images considering translations in $x$-axis using $t_x = 30$ and $-30$, and horizontal shearing using $s_h = 0.6$ and $-0.6$, respectively, and their registered versions using the proposed method. Corresponding results on the images *Room* and *Tree* considering translations in $x$-axis using $t_x = -20$ and 20, in $y$-axis using $t_y = -40$ and 40, and in rotation using $10^\circ$ clockwise and counterclockwise, respectively, are shown in Fig. 5. Visual assessments regarding the registration performance of the proposed method in the case of the image sets *Ship* and *CT-MRI* can be observed from Figs. 6 and 7, respectively. These figures show the reference-images, the sensed-images with distortion parameter values $t_x = 20$, $t_y = 40$, $\theta = 10^\circ$ clockwise for *Ship* and $t_y = -30$, $\theta = 10^\circ$ counterclockwise for *CT-MRI*, the corresponding registered-images, and the fused images obtained by combining the reference- and registered-images using a pixel-by-pixel maximization rule. From these figures, it may be seen that the proposed method is capable of providing registered-image that is visually aligned with the reference-image for multiple distortions in the sensed-image. Furthermore, the improved visual quality of the fused-images in Figs. 6 and 7 indicate that proper geometrical harmony is maintained in the reference- and registered-images.

The surface of the objective function on the $t_x s_h$-plane obtained in order to geometrically align the distorted versions of the images *Toy* and *MRI* using the proposed method is shown in Fig. 8. From this figure, it may be found that the proposed objective function possesses a good quality of smoothness, and as expected, the function converges to a minimum when $t_x = -30$ and $s_h = -0.6$ for the image *Toy*, and $t_x = 30$ and $s_h = 0.6$ for the image *MRI*. Similar results are obtained for the proposed objective function in the $t_x t_y$, $t_x\theta$, or $t_y\theta$ plane in order to register the images considered in the experiments, but are not shown to avoid redundancy in providing representative results.

Experiments are also carried out to evaluate the performance of the proposed registration method in aligning naturally distorted images available in real life. Figure 9 shows visual appearances of the images for such an example, wherein geometric alignment of two SAR images using the proposed method is considered. It may be seen from this figure that the scenes of the two images captured from the same geophysical location are different in terms of size as well as a rotational distortion remains among them. For the purpose of geometric alignment, the image having smaller scene is referred to as the reference-image and another as the sensed-image that possesses a counterclockwise rotational distortion. The variations of the objective function of the proposed method with respect to the clockwise rotation of the sensed-image is shown in Fig. 10. From this figure, it is seen that the objective function is minimized for a clockwise rotation at $\theta = 15^\circ$. The registered-image is obtained from the cropped and rotated version of the sensed-image, the scene of which may be overlaid on that of the reference-image, as shown in Fig. 9. Thus, the proposed registration method is capable of geometrically aligning naturally distorted images.

## 6 Conclusion

Development of an efficient and automatic image registration algorithm has become a potential area of research due to its numerous applications in image fusion and constructions of panoramic images and 3D scene. Due to a higher level of accuracy, intensity-based image registration algorithms are very often chosen in practice instead of feature-based methods. Approximate-level subband of a wavelet-like transform is commonly used for the development of computationally efficient intensity-based image registration algorithms. The directional selectivity of the transform and the objective function used for the image registration method play significant roles in providing a higher accuracy in the alignment process. Hence, in this paper, the curvelet transform that possesses

an improved directional selectivity as compared to many other wavelet-like transform and a new entropy-based objective function for the curvelet coefficients have been introduced for the development of an effective image registration algorithm. The proposed entropy-based objective function considers that conditional dependency may exist between the reference- and sensed-image to be registered. In order to calculate the conditional entropies, the approximate-level curvelet coefficients are statistically modeled using a locally i.i.d. bivariate Gaussian PDF. This statistical model for the curvelet coefficients of images has been verified by using the standard $\chi^2$-plot. In order to achieve a low level of computational burden for the proposed image registration method, a linear affine transformation is used for geometric alignment of the images that are distorted in common forms such as scaling, shearing, translations, and rotation. Extensive experimentations have been carried out on the synthetically distorted test images as well as naturally available misaligned images to evaluate the performance of the proposed method and compare with the existing methods. Comparisons of image registration performance in terms of commonly used metrics such as NRMSD, NCCC, and PRRMSE show that the proposed method is superior to the existing methods when the image to be registered have multiple forms of distortions. Thus, the proposed method is expected to play a significant role in automatic alignment of images in practice. There are a number of scopes to extend the research done in this paper. Some possible avenues include an integration of denoising algorithm for registration of noisy images, implementation of the registration algorithm considering nonlinear distortions such as the barrel or polynomial type and applying a general form of the PDF used for obtaining the objective function of the proposed algorithm.

## References


1. Arvalo, V., Gonzlez, J.: An experimental evaluation of non-rigid registration techniques on Quickbird satellite imagery. Int. J. Remote Sens. **29**(2), 513–527 (2008)
2. Suri, S., Reinartz, P.: Mutual-information-based registration of TerraSAR-X and Ikonos imagery in urban areas. IEEE Trans. Geosci. Remote Sens. **48**(2), 939–949 (2010)
3. Zhang, C., Fraser, C.P.: Automated registration of high-resolution satellite images. Photogramm. Rec. **22**(117), 75–87 (2007)
4. Wang, F., Vemuri, B.C.: Non-rigid multi-modal image registration using cross-cumulative residual entropy. Int. J. Comput. Vis. **74**(2), 201–215 (2007)
5. Ramprasad, P., Nagaraj, H.C., Parasuram, M.K., Shubha, M.: Multi resolution based image registration technique for matching dental X-rays. J. Mech. Med. Biol. **9**(4), 621–632 (2009)
6. Schmitt, O., Modersitzki, J., Heldmann, S., Wirtz, S.: Image registration of sectioned brains. Int. J. Comput. Vis. **73**(1), 5–39 (2006)
7. Wachinger, C., Navab, N.: Structural image representation for image registration. In: Proceedings of the IEEE Computer Society Conference on Computer Vision and Pattern Recognition Workshops, San Fransisco, pp. 23–30 (2010)
8. Zhaoying, L., Fugen, Z., Xiangzhi, B., Hui, W., Dongjie, T.: Multimodal image registration by mutual information based on optimal region selection. In: Proceedings of the IEEE International Conference on Information Networking and Automation, vol. 2, pp. 249–253. Kunming (2010)
9. Luo, B., Gan, J.-Y.: Inhomogenous illuminated images registration based on wavelet decomposition. In: Proceedings of the International Conference on Wavelet Analysis and Pattern Recognition, pp. 365–368. Baoding (2009)
10. Huang, J.-X., Li, D., Ye, F., Dong, Z.-J.: Flexible printed circuit defective detection based on image registration. In: Proceedings of the 3rd International Congress on Image and Signal Processing, pp. 2570–2574. Yantai (2010)
11. Brown, M., Lowe, D.G.: Automatic panoramic image stitching using invariant features. Int. J. Comput. Vis. **74**(1), 59–73 (2007)
12. Suh, J.W., Wyatt, C.L.: Registration under topological change for CT colonoscopy. IEEE Trans. Biomed. Eng. **58**(5), 1403–1411 (2011)
13. Kim, J., Fessler, J.A.: Intensity-based image registration using robust correlation coefficients. IEEE Trans. Med. Imaging **23**(11), 1430–1444 (2004)
14. Ghantous, M., Ghosh, S., Bayoumi, M.: A multi-modal automatic image registration technique based on complex wavelets. In: Proceedings of the 16th IEEE International Conference on Image Processing, Cairo, pp. 173–176 (2009)
15. Corsini, M., Dellapiane, M., Ponchio, F., Scopigno, R.: Image-to-geometry registration: a mutual information method exploiting illumination-related geometric properties. Comput. Graph. Forum **28**(7), 1755–1764 (2009)
16. Maes, F., Collignon, A., Vandermeulen, D., Marchal, G., Suetens, P.: Multimodality image registration by maximization of mutual information. IEEE Trans. Med. Imaging **16**(2), 187–198 (1997)
17. Qin, B., Gu, Z., Sun, X., Lv, Y.: Registration of images with outliers using joint saliency map. IEEE Signal Process. Lett. **17**(1), 91–94 (2010)
18. Malviya, A., Bhirud, S.G.: Wavelet based image registration using mutual information. In: Proceedings of the International Conference on Emerging Trends in Electronic and Photonic Devices and Systems, pp. 241–244. Varanasai (2009)
19. Shi, H., Luo, S.: Image registration using the shift-insensitive discrete wavelet transformation. In: Proceedings of the International Conference on Medical Image Analysis and Clinical Applications, pp. 46–49. Guangdong (2010)
20. Ton, J., Jain, A.K.: Registering landsat images by point matching. IEEE Trans. Geosci. Remote Sens. **27**(5), 642–651 (1989)
21. Heo, J., Kim, J.H., Eo, Y.D., Sohn, H.-G.: Automated TM/ETM+ image co-registration using pre-qualified area matching and studentized outlier detection. Imaging Sci. J. **57**(2), 69–78 (2009)
22. Habib, A.F., Al-Ruzouq, R.I.: Semi-automatic registration and change detection using multi-source imagery with varying and radiometric properties. Photogramm. Eng. Remote Sens. **71**(3), 325–332 (2005)
23. Kwak, T.-S., Kim, Y.-I., Yu, K.-Y., Lee, B.-K.: Registration of aerial imagery and aerial LiDar data using centroids of plane roof surfaces as control information. KSCE J. Civ. Eng. **10**(5), 365–370 (2006)
24. Ryan, N., Heneghan, C., de Chazal, P.: Registration of digital retinal images using landmark correspondence by expectation maximization. Image Vis. Comput. **22**, 883–898 (2004)
25. Lu, G., Yan, J., Kou, Y., Zhang, J.: Image registration based on criteria of feature point pair mutual information. IET Image Process. **5**(6), 560–566 (2011)
26. Gonzalez, R. C., Woods, R. E.: Digital Image Processing. 2nd edn. Pearsons, Singapore (2002)

27. Szeliski, R.: Computer Vision Algorithms Applications. Springer, New York (2011)
28. Yang, Z., Shen, G., Wang, W., Qian, Z., Ke, Y.: Spatial-spectral cross correlation for reliable multispectral image registration. In: Proceedings IEEE Applied Imagery Pattern Recognition Workshop, pp. 1–8. Washington, DC (2009)
29. Kaplan, L.M., Nasrabadi, N.M.: Block Wiener-based image registration for moving target indication. Image Vis. Comput. **27**, 694–703 (2009)
30. Gao, Z., Gu, B., Lin, J.: Monomodal image registration using mutual information based methods. Image Vis. Comput. **26**, 164–173 (2008)
31. Du, Q., Chen, L.: An image registration method based on wavelet transform. In: Proceedings of the International Conference on Computer, Mechatronics, Control and Electronic Engineering, Changchun, pp. 158–160 (2010)
32. Peng, X., Wei, B., Chen, Q.: An efficient image registration method based on mutual information model. In: Proceedings of the 7th International Conference on Fuzzy Systems and Knowledge Discovery, pp. 2168–2172. Yantai, Shandong (2010)
33. Wells, W.M., Viola, P., Atsumi, H., Nakajima, S., Kikinis, R.: Multi-modal volume registration by maximization of mutual information. Med. Image Anal. **1**(1), 35–51 (1996)
34. Zhu, Y.-M.: Volume image registration by cross entropy optimization. IEEE Trans. Med. Imaging **21**(2), 174–180 (2002)
35. Neemuchwalaa, H., Heroa, A., Carsona, P.: Image matching using alpha-entropy measures and entropic graphs. Signal Process. **89**, 724–737 (2009)
36. Gholipour, A., Kehtarnavaz, N., Yousefi, S., Gopinath, K., Briggs, R.: Symmetric deformable image registration via optimization of information theoretic measures. Image Vis. Comput. **28**, 965–975 (2010)
37. Balakrishnan, N., Lai, C.-D.: Continuous Bivariate Distributions. Springer, New York (2009)
38. Mallat, S.: A Wavelet Tour of Signal Processing, 2nd edn. Academic Press, San Diego (1999)
39. Peter, A.M., Rangarajan, A.: Maximum likelihood wavelet density estimation with applications and shape matching. IEEE Trans. Image Process. **17**(4), 458–468 (2008)
40. Hongli, S., Bo, H.: Image registration using a new scheme of wavelet decomposition. In: Proceedings of the IEEE Conference on Instrumentation and Measurement Technology, pp. 235–239. Victoria, BC (2008)
41. Gao, X.Q., Nguyen, T.Q., Strang, G.: A study of two-channel complex-valued filter banks and wavelets with orthogonality and symmetry properties. IEEE Trans. Signal Process. **50**(4), 824–833 (2002)
42. Kingsbury, N.G.: Image processing with complex wavelets. Philos. Trans. Soc. Lond. Appl. Math. Phys. Sci. **357**(1760), 2543–2560 (1999)
43. Candes, E.J.: Harmonic analysis of neural networks. Appl. Comput. Harmon. Anal. **6**(2), 197–218 (1999)
44. Candes, E.J., Donoho, D.L.: Ridgelets: a key to higher-dimensional intermittency? Philos. Trans. Soc. Lond. Appl. Math. Phys. Sci. **357**(1760), 2495–2509 (1999)
45. Candes, E.J., Donoho, D.L.: Curvelets—a surprisingly efffective nonadaptive representation for objectives with edges. In: Cohen, A., Rabut, C., Schumaker, L. (eds.) Curves and Surface Fitting: Saint-Malo 1999. Vanderbilt University Press, Nashville (2000)
46. Candes, E.J., Donoho, D.L.: New tight frames of curvelets and optimal representations of object with piecewise $\mathcal{C}^2$ singularities. Commun. Pure Appl. Math. **57**(2), 219–266 (2004)
47. Demanet, L., Ying, L.: Curvelets and wave atoms for mirror-extended images. In: Proceedings of the SPIE Wavelets XII, vol. 6701, p. 67010J. San Diego (2007)
48. Chauris, H., Nguyen, T.: Seismic demigration/migratoin in the curvelet domain. Geophysics **73**(2), 4203–4215 (2005)
49. Choi, M., Kim, R.Y., Nam, M.-R., Kim, H.O.: Fusion of multispectral and panchromatic satellite images using the curvelet transform. IEEE Geosci. Remote Sens. Lett. **2**(2), 136–140 (2005)
50. Ma, J., Plonka, G.: The curvelet transform: a review of recent applications. IEEE Signal Process. Mag. **27**(2), 118–133 (2010)
51. Liu, J., Moulin, P.: Information-theoretic analysis of interscale and intrascale dependencies between image wavelet coefficients. IEEE Trans. Image Process. **10**(11), 1647–1658 (2001)
52. Rahman, S.M.M., Hasan, M.K.: Wavelet-domain iterative center weighted median filter for image denoising. Signal Process. **83**, 1001–1012 (2003)
53. Roy, S., Howlader, T., Rahman, S.M.M.: Image fusion technique using multivariate statistical model for wavelet coefficients. Signal, Image and Video Processing (published online) (2011). doi:10.1007/s11760-011-0241-9
54. Rahman, S.M.M., Ahmad, M.O., Swamy, M.N.S.: Video denoising based on inter-frame statistical modeling of wavelet coefficients. IEEE Trans. Circuits Syst. Video Technol. **17**(2), 187–198 (2007)
55. Howlader, T., Chaubey, Y.P.: Noise reduction of cDNA microarray images using complex wavelets. IEEE Trans. Image Process. **19**(8), 1953–1967 (2010)
56. Rahman, S.M.M., Ahmmad, M.O., Swamy, M.N.S.: Statistics of 2-D DT-CWT coefficients for a Gaussian distributed signal. IEEE Trans. Circuits Syst. I Regul. Pap. **55**(7), 2013–2025 (2008)
57. Everitt, B.S., Skrondal, A.: The Cambridge Dictionary of Statistics, 4th edn. Cambridge University Press, New York (2010)
58. Cover, T.M., Thomas, J.A.: Elements of Information Theory, 2nd edn. Wiley, New Jersey (2006)
59. Ahmed, N.A., Gokhale, D.V.: Entropy expressions and their estimators for multivariate distributions. IEEE Trans. Inf. Theory **35**(3), 688–692 (1989)
60. Lazo, A.V., Rathie, P.: On the entropy of continuous probability distributions. IEEE Trans. Inf. Theory **24**(1), 120–122 (1978)
61. Mekky, N.E., Abou-Chadi, F.E., Kishk, S.: A new dental panoramic X-ray image registration technique using hybrid and hierarchical strategies. In: Proceedings of the International Conference on Computer Engineering and Systems, pp. 361–367. Cairo (2010)
62. Beaulieu, M., Foucher, S., Gagnon, L.: Multi-spectral image resolution refinement using stationary wavelet transform. In: Proceedings of the IEEE International Geosciences and Remote Sensing Symposium, vol. 6, pp. 4032–4034. Toulouse (2003)